Effect of bond in the development length of CFRP pretensioned beams

Eleni Toumpanaki [1], Janet M. Lees [2]

[1]Department of Architecture, [2]Engineering Department, University of Cambridge, Cambridge, UK

Giovanni P. Terrasi

Swiss Federal Laboratories for Materials Science and Technology (EMPA), Laboratory for Mechanical Systems Engineering, Dübendorf , Switzerland

Contacting author: et343@cam.ac.uk

Abstract

Carbon Fibre Reinforced Polymer (CFRP) tendons present an alternative material that can mitigate steel corrosion problems in concrete bridges. The use of CFRP prestress tendons can result in more durable prestressed concrete structures. However, the potential matrix plasticisation of CFRP tendons in humid environments and their inherent lack of ductility need to be considered in the design process. A tension stiffening analysis is undertaken to study the effect of variations in bond strength parameters on the cracking behaviour, deformability and structural performance of CFRP prestressed beams. The bond strength scenarios under consideration reflect either low or high bond conditions. The former could be associated with epoxy plasticisation and bond degradation due to moisture ingress at a crack location. A low bond performance results in a smaller number of cracks and higher deflections at failure compared with high bond tendons.

Keywords: Composites, Concrete, Long-term effects, Durability, Deformability

1. Introduction

Incidents of severe corrosion in steel prestressing tendons have been reported in structural applications such as bridges (e.g. Hammersmith Flyover [1]). The FHWA (Federal Highway Administration) has estimated that the annual direct cost estimate of steel corrosion in highway bridges is $8.3 billion dollars [2] and £200 million has been invested by TFL for the strengthening and repair of bridges and tunnels [3]. Due to the encasement of the steel tendons in concrete, inspection of internal steel tendons can be difficult. Concrete cracks act as paths for corrosive materials and can be a sign of construction deficiencies and impending corrosion problems. Steel corrosion can lead to high repair and maintenance costs and traffic disruption problems and, in extreme cases, to catastrophic brittle failures (e.g. Genoa Bridge 2018 [4]). Steel corrosion can be particularly critical in prestressed structures, where the tendons are loaded up to 70% of their ultimate tensile strength. This leaves a limited margin for any increase in steel stress as a result of a reduction in the effective cross-sectional area due to corrosion.

Carbon Fibre Reinforced Polymer (CFRP) tendons present an alternative material that can mitigate steel corrosion problems. The corrosion-free nature of CFRP can result in an enhanced durability performance for prestressed concrete structures. CFRPs exhibit a high strength to weight ratio, are easy to handle, have lower transportation costs and are suitable for structural applications near high voltage cables and in MRI rooms in hospitals due to their electromagnetic neutrality. However, the matrix resin component of CFRP tendons plasticises when exposed to humid conditions (e.g. at a crack location) and FRPs exhibit linearly elastic brittle failures. The effect of environmental conditions on the long-term mechanical performance of FRPs has been considered in ACI guidelines [5] through the use of an environmental reduction factor applied to the design tensile strength. However, humid environments also affect more matrix-dominated properties such as the bond, shear and dowel strength of FRPs. ACI guidelines [5] refer to existing literature for the long-term bond durability performance of FRPs and suggest that durability factors should be obtained by the manufacturer. The latter advice reflects the lack of standardisation in FRP materials. The chemical structure of resins is usually proprietary and resin formulations are constantly being developed in industry [6] hindering quantitative recommendations for long-term effects.

Epoxy-dominated bond failure mechanisms in CFRP tendons and any deterioration in the epoxy-dominated mechanical properties of CFRPs in humid and alkaline environments need to be accounted for when assessing the durability performance of CFRP prestressed structures [7]. This is of particular interest when cracked FRP prestressed structures (partial prestressing conditions) are in high humidity environments and subjected to temperature fluctuations. The bond between CFRP tendons and concrete is important in pretensioned structures to safely transfer the prestressing force to the concrete. When a crack forms the stresses from the FRP tendon are transferred to the concrete through bond and tension stiffening occurs. Therefore, the bond stress-slip relationship can affect the deformability and failure of prestressed structures. Any degradation of the bond strength in the anchorage zone can result in a reduction of the effective prestress force and an increase in the transfer length. If an adequate transfer length is not provided, the load carrying capacity of the member can decrease. Even if an adequate transfer length is initially provided, degradation of the bond strength in the vicinity of cracks in the flexural development length can result in a premature debonding failure that encroaches on the transfer length. Thus slippage of the tendon takes place and the structural capacity decreases. A similar type of debonding failure in CFRP sand coated tendons has been experimentally reported in [8].

Bond can also play an important role in the deformability of FRP prestressed concrete structures. A high deformability is usually preferred in CFRP prestressed structures in order to enhance the warning before collapse. Deformability can often be misinterpreted as ductility due to conventional steel-based definitions of ductility indices that rely on ratios of deformability variables, such as rotation, deflection and curvature, at failure to the respective ones at first yield. But FRPs do not yield and have a lower Young's modulus. The energy stored in FRP prestressed concrete structures is mostly elastic that can be released upon the sudden removal of loading leading to potential damage. Naaman and Jeong [9] tried to distinguish between deformability and ductility by introducing an energy-based ductility index. This is based on the total energy stored under the load-displacement curve and the elastic energy released upon unloading. The work showed distinctive differences in ductility between steel and FRP prestressed concrete beams. ISIS [10] has introduced a deformability factor based on the moment and curvature at the limit state and serviceability state and recommended a value of at least 4 to ensure adequate deformation before failure to avoid brittle collapse.

The purpose of this study is to investigate two distinctive bond stress-slip scenarios, representative of low and high bond tendons, on the cracking behaviour, ultimate failure and deformability of CFRP prestressed beams. A numerical analysis with a refined section by section methodology is carried out to account for tension stiffening effects and to explore the influence of

bounds of bond stress-slip behaviour that reflect CFRP sand coating variability and environmental exposure, as experimentally found in [11].

2. Numerical Analysis

To study the effect of variations in the bond stress-slip behaviour on the cracking behaviour and beam deformability, a simply supported beam with a span L=2.50 m and prestressed with two CFRP tendons of diameter D=5.4 mm at the same depth is considered. An initial prestress force of 40%f_{tu}, where f_{tu} is the ultimate tensile strength of the CFRP tendon and a 3 point loading configuration are assumed (Figure 1b). Details of the beam cross section are shown in Figure 1a. High strength concrete is used and the transfer length L_t calculated based on ACI 440.4R-04 [12] varies from 49-124 mm depending on the adopted bond coefficient. The transfer length has been found experimentally to be less than 160 mm for similar CFRP tendons and a prestressing ratio of less than 60% [13]. In this analysis a transfer length of 135 mm is assumed.

2.1 Material Properties

The mechanical properties of the materials used in this study are summarised in Table 1. To account for long-term effects of creep and shrinkage, the effective concrete elastic modulus was calculated using

$$E_{c,eff}(t,t_o)=E_c/(1+\varphi) \quad (1)$$

It is assumed that the compressive concrete failure strain is independent of the time under load in accordance with [14]. However, creep affects the strains within the elastic range and therefore the tensile concrete failure strain. For concrete in compression the concrete model proposed in [15] is adopted,

$$\sigma_c=f_{cu}-f_{cu}\left(1-\varepsilon_c/\varepsilon_{cu}\right)^{nheld} \quad (2)$$

where $nheld=E_c\varepsilon_{cu}/f_{cu}$, σ_c is the concrete stress associated with a concrete strain ε_c, f_{cu} is the ultimate compressive strength and ε_{cu} is the ultimate compressive strain. This model has been shown to be applicable for high strength concrete [16]. By considering the effective concrete elastic modulus $E_{c,eff}(t,t_o)$ in the *nheld* term, a concave shape is exhibited at $\varepsilon_c \geq 0.0025$ instead of a convex shape that is representative of the concrete behaviour. Therefore, the Held model was applied for $\varepsilon_c \leq 0.0025$. For $0.0025<\varepsilon_c<0.0030$ the Young's modulus was assumed to vary linearly between E_c=22-27GPa and a plastic concrete stress distribution was adopted for $0.0030\leq\varepsilon_c\leq 0.0035$.

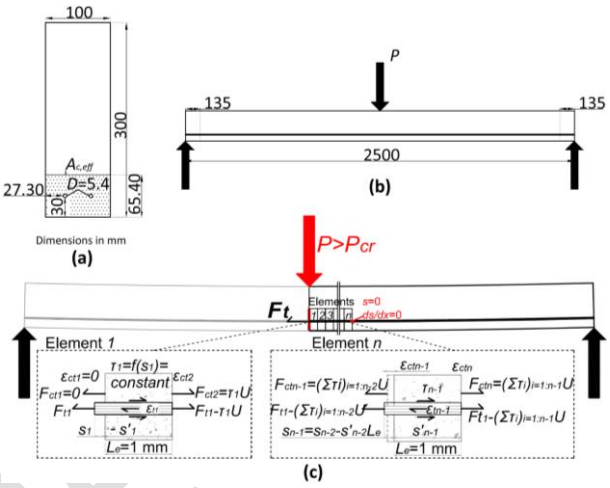

Figure 1. (a) Beam section, (b) Load configuration and (c) Numerical analysis method

Table 1. Material properties

CFRP tendon	
Ultimate tensile strength, f_{tu} (MPa)	1913
Longitudinal elastic modulus, E_L (GPa)	150
Ultimate tensile strain, ε_{tu} (MPa)	0.016
Volume fraction, V_f	0.64
High strength concrete	
Concrete compressive cube strength, f_{cu} (MPa)	100
Concrete tensile strength, f_{ctu} (MPa)	5.20
Ultimate concrete compressive strain, ε_{cu}	0.0035
Ultimate concrete tensile strain, ε_{ctu}	0.00014
Concrete elastic modulus, E_c (GPa)	36.50
Autogeneous and drying shrinkage strain,	0.0004
Creep coefficient, φ	1.0

2.2 Methodology

To study the post-cracking flexural behaviour of

the prestressed concrete beam, a numerical solution with a refined section by section analysis is implemented by considering the bond stress-slip behaviour of the CFRP tendons [17]. The first crack is assumed to occur at the mid-span (point of maximum moment M_{max}). To predict the position of the next crack two regions are defined along the beam based on the slip boundary conditions. The partial interaction (PI) region is a zone where slip takes place ($s \neq 0$ and $ds/dx \neq 0$) and there is a tension stiffening effect. The full interaction region (FI) is the length over which there is no relative slip between the tendon and the concrete. There is therefore full composite action and an elastic uncracked analysis is applied. The next crack can form either in a partial or a full interaction region. In the PI region the concrete tensile strain capacity is exceeded either from the developed bond stresses or the sectional concrete strain distribution that equilibrates the applied moment. In the FI region cracking takes place where the applied moment $M(x)$ exceeds the elastic cracking moment M_{cr}. In the partial interaction region, an iterative procedure is followed for a given tendon strain value, ε_{t1}, at the crack location (x=0). Slip values, s_1, are assumed until the boundary conditions of zero slip s and zero 'slip-strain' ds/dx (full interaction condition) are satisfied at the end of the transfer length l_t. To account for the long-term effects of creep and shrinkage, the 'slip-strain' is given by

$$s' = {ds}/{dx} = (\varepsilon_t - \varepsilon_{t\text{-}pre}) - (\varepsilon_{ct} - \varepsilon_{csh} - \varepsilon_{cc} - \varepsilon_{c\text{-}pre}) \quad (3)$$

where ε_t is the tendon strain, $\varepsilon_{t\text{-}pre}$ is the tendon strain due to the prestressing force subtracted by the concrete elastic shortening, ε_{ct} is the concrete tensile strain, ε_{csh} is the concrete shrinkage (autogeneous and drying), ε_{cc} is the concrete creep strain and $\varepsilon_{c\text{-}pre}$ is the concrete compressive strain from the applied prestressing force at the tendon level.

The transfer length, l_t, is discretised into smaller elements of L_e=1.0 mm. For a given slip value s_1, the bond stress at the first element $\tau_1 = f(s_1)$ is calculated based on the specific bond stress-slip law considered and is assumed to be constant along each element. The total bond force acting over the first segment $\tau_1 U$ (where $U = \pi D L_e$) is transferred to the concrete effective area of the second element as tension F_{ct2} and the force of the tendon at the end of the first segment is reduced by $\tau_1 U$, $F_{t2} = F_{t1} - \tau_1 U$. The concrete and tendon strain values, ε_{ct2} and ε_{t2} respectively, can be derived based on the forces F_{ct2} and F_{t2} divided by $E_c A_{c,eff}$ and $E_t A_t$ for the concrete and tendon respectively. The slip of the second element s_2 is calculated by subtracting $(ds/dx)_1 L_e$ from the assumed slip s_1. These values are considered as input values for the analysis of the second element and the above process is repeated until the boundary conditions are met at l_t (Equations 4 and 5 and Figure 1c).

$$s_{n-1} = s_{n-2} - s'_{n-2} L_e = 0 \quad (4)$$

$$s'_{n-1} = 0 \quad (5)$$

where n is the last element of the discretised length l_t and in Equation 3 and 5 $\varepsilon_t = \varepsilon_{tn-1} = (F_{t1} - \sum_{i=1}^{n-1} \tau_i U) / A_{c,eff}$.

Here, an effective concrete area, $A_{c,eff}$, (shaded area in Figure 1a) with $h_{eff} = 2c + D$ is adopted according to [17] to account for tension stiffening. This technique has been previously adopted for the analysis of tension stiffening effects under static monotonic [17] and cycling loading [18] resulting in a good agreement with experimental results.

The moment capacity at each crack location is calculated based on a direct cross-sectional analysis, where the concrete strain at the compressive fibre is assumed and an iterative procedure is followed until equilibrium of the internal forces is satisfied. This is based on the assumptions that 'plane sections remain plane', there is a strain compatibility between the change in the tendon strain and the top concrete compressive strain, and concrete does not contribute in tension [19] (see Figure 2a). However, the strain compatibility approach between the tendon and the concrete is violated where debonding takes place, or low bond tendons are used. In this case a rigid body analysis is more appropriate where the concrete deformation at the compressive fibre is calculated based on the slip values at the tendon layer. The strain in the top concrete fibre can be theoretically estimated by dividing the contraction, δ_c, by a certain length, L_{eff} (see Figure 2b). The choice of the effective length,

L_{eff}, is debatable and here it is considered to be half the crack spacing [17]. To identify the threshold where the strain compatibility or the rigid body analysis becomes a more appropriate representation, a unified method is proposed. This is important, if a tendon failure, as calculated from a strain compatibility approach, can be impeded due to high tendon slip values (low bond tendons or debonding) and high crack rotations lead to a concrete failure and a potential increase in the moment and curvature capacity of the beam. The criterion adopted here to invoke a rigid body analysis is when the rotation of a rigid block $\theta_{sb}=s_1/(d\text{-}xg_1)$ exceeds the rotation $\theta_{cb}=(\varepsilon_c/xg_1)L_{eff}$, as calculated based on a strain compatibility approach where xg_1 is the neutral axis at the first crack at the mid-span and d is the depth of the beam.

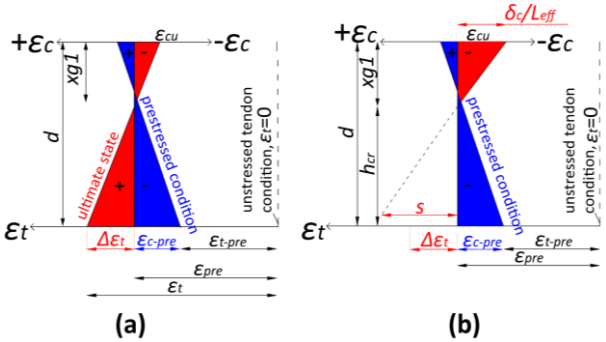

Figure 2. (a) Strain compatibility sectional analysis and (b) Rigid body sectional analysis.

2.3 Bond stress-slip models

Two distinctive bond stress-slip scenarios indicative of low and high bond tendons are studied (LE-LB and LE-HB). The adopted bond stress-slip models were the mB.E.P. (modified Bertero, Eligehausen and Popov model) and a linear frictional model for the ascending and descending branch respectively. The bond parameters of each model are summarised in Table 2 and were derived from an experimental series presented in [11].

The differences in the τ_m values between the LE-HB and LE-LB bond scenarios represent material variability between CFRP sand coated tendons of the same manufacturing pultrusion line as experimentally observed in [20]. However, the LE-HB bond scenario could also reflect durability effects and localised swelling phenomena due to moisture uptake at the vicinity of a crack in FRP prestressed concrete beams in combination with concrete shrinkage effects that are more pronounced in early age concrete. At longer exposure times, where matrix plasticisation and degradation dominate, a LE-LB scenario becomes more applicable.

Table 2. Bond stress-slip scenarios of the parametric study

		LE-HB	LE-LB
mB.E.P. $\tau=\tau_m\left(\frac{s}{s_m}\right)^{\alpha}$; $s\le s_m$	τ_m	19.23	6.15
	s_m	0.40	0.11
	α	1.00	0.79
Linear frictional $\tau=\tau_{fr}\text{-}p'(s\text{-}s_m)$; $s>s_m$	τ_{fr}	8.08	4.87
	p'	0.31	0.13

Note: LE: long-term effects (creep and shrinkage), HB: high bond strength τ_m and LB: low bond strength τ_m.

3. Analytical results

The moment at the decompression stage (zero tensile strain at the bottom fibre) and at first cracking accounting for long-term effects are M_{dec}= 6.32 kNm and M_{cr}=15.13 kNm respectively based on an elastic analysis. The beam is under-reinforced with a ρ=0.17% < ρ_b=0.77% in order to investigate the contribution of the rotational capacity due to debonding on the failure mode. The ultimate moment due to tendon rupture is M_u=26.97 kNm. Figure 3 shows the formation of the second crack and the cracking pattern at the ultimate failure in half of the beam for both bond stress-slip scenarios LE-HB and LE-LB. The applied moments, the tendon strain as derived by the numerical analysis described above, the crack width and the crack rotation θ_{sb} at a distance x from the first crack at mid-span are also depicted in Figure 3. The crack width, w, at the tendon layer is derived from the sum of the slip values at the right and left side of each crack. Primary cracks are those formed in the full interaction region and secondary cracks are those formed from the build-up of the bond stresses.

The second crack in LE-HB forms at a lower moment M_{max}=19.05 kNm in the full interaction region and at a smaller spacing when compared with LE-LB. This is the result of the high bond

strength τ_m that resulted in a smaller transfer length l_t for a given tendon strain in LE-HB. In LE-LB debonding takes place at an early stage due to the bond stress-slip model as the transfer of the bond stresses relies mostly on the frictional bond component. In LE-LB the formation of the second and third crack due to the build-up of bond stresses and the elastic cracking moment respectively take place at a tendon strain value 9% higher than in LE-HB and the debonding length is extended by up to 160 mm from the first crack (Figure 4). At failure, 5 cracks and 3 cracks are fully developed in the LE-HB and LE-LB beams respectively. A 6th crack might form at x=407 mm at failure in LE-HB due to the build-up of bond stresses. The 3rd and 5th crack in LE-HB and the 2nd crack in LE-LB developed in the partial interaction region. The primary crack spacing is estimated to be 260 mm in LE-HB and 345 mm in LE-LB. The crack widths and crack rotations in LE-LB are consistently higher than in LE-HB. Yet, the θ_{sb} rotations did not exceed the θ_{sc} rotations in the LE-LB scenario and a rigid body analysis was therefore not applied based on the unified approach described above. Both beams fail by tendon rupture. The flexural bond length at tendon rupture is higher in LE-HB (L_f=713 mm) than in LE-LB (L_f=623 mm) and this is attributed to the higher number of cracks developed in the former case and the fact that the 4th crack formed at x=519 mm due to exceedance of the elastic cracking moment. The flexural bond length at failure is adequate and the partial interaction region does not extend up to the transfer length of the prestressing force. This holds even if we consider an increase in transfer length by 40%, up to L_t=189 mm, as observed elsewhere due to creep and shrinkage effects [21].

In Figure 5 the predicted load versus deflection behaviour is plotted for both the LE-LB and LE-HB bond scenarios in the CFRP prestressed beam studied here. The deflections were derived from the curvature of the uncracked concrete sections in the full interaction region and the crack rotations θ_{sb} in the partial interaction region by carrying out numerical integration. To compare, load-deflection plots are included by applying an effective moment of inertia, I_{eff}, as found in [12] and in [22] for FRP prestressed concrete. The I_{eff} was considered only in the partial interaction region.

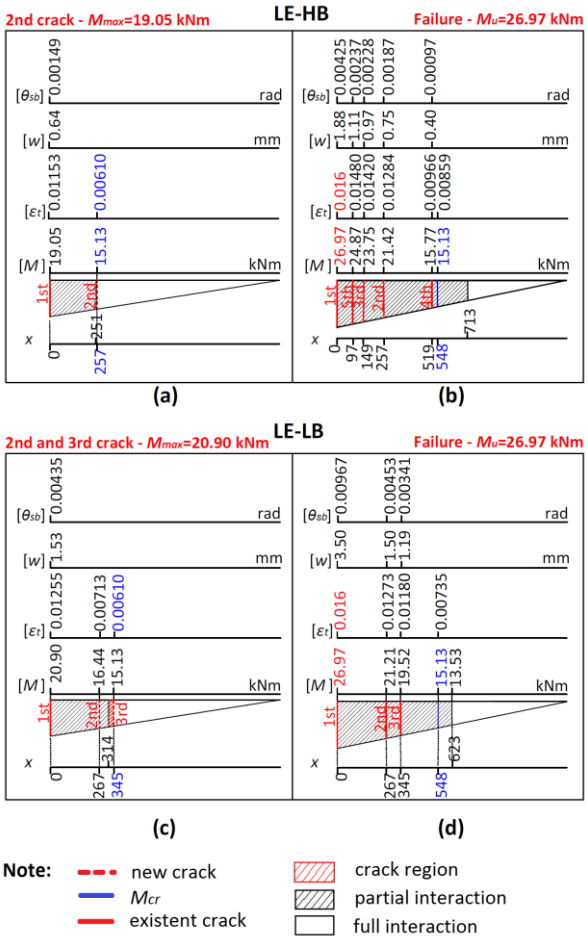

Figure 3. Crack formation stage in LE-HB (a) M_{max}=19.05 kNm, (b) M_u=26.97 kNm and in LE-LB (c) M_{max}=20.90 kNm and (d) M_u=26.97 kNm.

At the same failure load the LE-LB scenario results in a 50% increase in the ultimate deflection compared with LE-HB. The ACI 440.4R-04 [12] approach and the Bischoff [22] effective moment of inertia, I_{eff}, approach agree well with high bond (LE-HB) and low bond (LE-LB) tendons respectively. The ductility indices according to [9] for the LE-HB and LE-LB beams are μ=3.10 and μ=4.0 respectively. The deformability factor according to [10] is 119 following a strain compatibility approach for the calculation of the curvature.

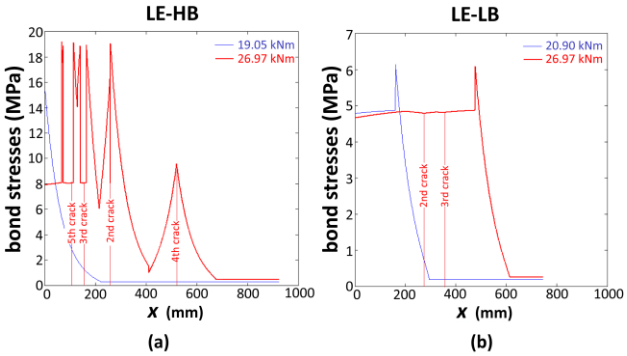

Figure 4. Bond stresses along the development length for (a) LE-HB and (B) LE-LB.

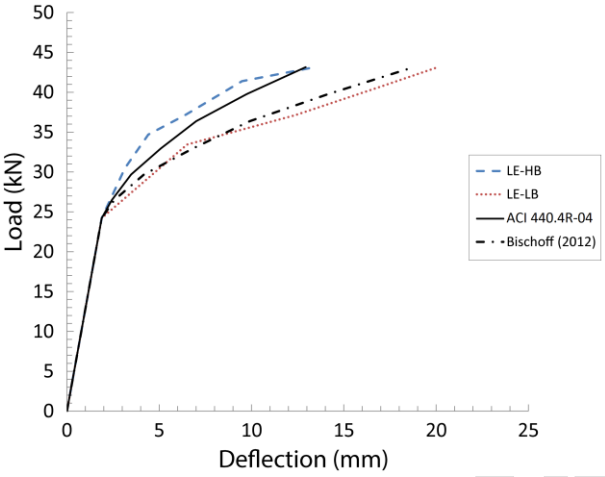

Figure 5. Load-deflection plot.

4. Discussion

The unified approach proposed in section 2.2 seems more appropriate at higher tendon ratios closer to the balanced tendon ratio, where failure modes can shift from tendon rupture to concrete crushing. A rigid body analysis could not be applied for the specific tendon ratio studied here. Yet, the resulting analytical θ_{sb} rotations (see Figure 3) would result in concrete crushing for the given crack spacing.

In FRP structures it is common to use deformability as a measure of an impending failure. Yet, the proposed factors in [9] and [10] are rather different. Agreement between design guidelines needs to be established. The ductility index, μ, in [9] is more appropriate because it reflects the energy dissipation due to the concrete crack formation stage, the inelastic concrete deformation and bond frictional losses and the elastic energy released at failure. The latter is significant in FRP pretensioned structures due to the lack in ductility in FRPs and in order to understand potential catastrophic failure upon release of the stored elastic energy. Low bond tendons exhibit higher deformability but the higher number of cracks in a CFRP pretensioned beam with high bond tendons can act as a warning of distress.

The shear span to effective depth ratio of the CFRP pretensioned beam is 4.2 and the deflections were calculated based on [12] and [22] and the slip values at the tendon level. Shear deformations and the additional rotation due to the development of shear cracking at higher loads are neglected. Shear induced deformations are expected to be dominant in the vicinity of the supports. Experimental results in [23] showed that the development of diagonal cracking at initially formed flexural cracks can increase the total deflection by up to 30%. A further development of the analytical model studied here should include the effect of shear crack propagation and rotation on the behaviour and total deflection of CFRP pretensioned beams.

5. Conclusions

A low bond performance that could be indicative of a reduction in bond properties due to long-term exposure in humid conditions exhibited a smaller number of cracks and higher deflections at failure compared with high bond tendons. Debonding failures of the tendons in the anchorage zone were not observed. Warning of pending collapse can be enhanced either through a high deformability in beams with low bond tendons or an increased number of cracks in beams with high bond tendons. In both cases energy dissipation is provided through the inelastic concrete deformation and crack formation.

6. Acknowledgements

We are grateful to SACAC Ltd for their technical and financial support. The financial support from the Onassis Foundation (ET) is also greatly appreciated.

7. References

[1] Lynch, D. Hammersmith flyover: returning to full strength. *New Civil Engineer*. 2012; 98: 14-16.

[2] Gerhardus, H.K., Michiel, P.H.B., Neil, G.T., Virmani, Y.P., and Payer, J.H. Corrosion costs and preventive strategies in the United States. Report FHWA-RD-01-156, NACE; 2002.

[3] Hansford, M. Costain with Hammersmith job. *New Civil Engineer*. 2013.

[4] Glanz, J. Pianigiani, G., White, J. and Patanjali, K. Genoa Bridge Collapse: The Road to Tragedy. *New York Times*. 2018.

[5] ACI 440.1R-15. Guide for the Design and Construction of Structural Concrete Reinforced with Fiber-Reinforced Polymer (FRP) Bars. American Concrete Institute, Farmington Hills, MI, USA; 2015.

[6] Lees, J.M., Toumpanaki, E., Barbezat, M. and Terrasi, G.P. Mechanical and durability screening test methods for cylindrical CFRP prestressing tendons. *Journal of Composites for Construction.* 2017; **21**(2): 13p.

[7] Toumpanaki, E., Lees, J.M. and Terrasi, G.P. Shear modulus of cylindrical CFRP tendons exposed to moisture. *Journal of Composites for Construction.* 2014; **19**(3): 12p.

[8] Terrasi, G.P., Meier, U. and Affolter, C. Long-term bending creep behavior of thin-walled CFRP tendon pretensioned spun concrete poles. *Polymers*. 2014; **6**(7): 2065-2081.

[9] Naaman, A.E., and Jeong S.M. Structural ductility of concrete prestressed with FRP tendons. *Proc., 2nd Int. Symp. on Non-Metallic (FRP) Reinforcement for Concrete Structures (FRPRCS-2)*, *Ghent*; 1995: 379-386.

[10] ISIS Canada. Reinforcing concrete structures with fiber-reinforced polymers-Design manual No.3, Manitoba, Canada: ISIS Canada Corporation; 2001.

[11] Toumpanaki, E. Durability and bond performance of CFRP tendons in high strength concrete. Ph.D. thesis, Department of Engineering, University of Cambridge; 2015.

[12] ACI 440.4R-04 Prestressing Concrete Structures with FRP Tendons, American Concrete Institute, Farmington Hills, MI, USA; 2011.

[13] Terrasi, G.P., Bisby, L., Barbezat, M., Affolter, C., and Hugi, E. Fire behavior of thin CFRP pretensioned high-strength concrete slabs. *Journal of Composites for Construction*. 2012; **16**(4): 381–394.

[14] Deskovic, N., Meier, U., and Triantafillou, T.C. Innovative design of FRP combined with concrete: long-term behaviour. *Journal of Structural Engineering.* 1995; **121**(7): 1079-1089.

[15] Held M. A contribution to the manufacture and dimensioning of high strength concrete compressive members. Ein Beitrag zur Herstellung und Bemessung von Druckgliedern aus hochfestem Normalbeton (B60-B125) (in German). Ph.D. Thesis, Department of Structural Engineering, TU Darmstadt; 1992.

[16] Terrasi, G.P. Spun Concrete Poles Pretensioned with CFRP Tendons. Mit Kohlenstoffasern vorgespannte Schleuderbetonrohre (in German). Ph.D. Thesis, ETH Zurich, Switzerland; 1998.

[17] Knight, D., Visintin, P., Oehlers, D., and Mohamed Ali, M. Short-term partial-interaction behavior of RC beams with prestressed FRP and steel. *Journal of Composites for Construction*. 2014; **18**(1): 1–9.

[18] Zanuy, C., Albajar, L., and de la Fuente, P. On the cracking behaviour of the reinforced concrete tension chord under repeated loading. *Materials and Structures*. 2009; **43**(5): 611–632.

[19] Eurocode 2 (EC2). Design of concrete structures-Part 1-1: General rules and rules for buildings. ENV 1992-1-1:2004, Brussels, Belgium; 2004.

[20] Toumpanaki, E., Lees, J.M. and Terrasi, G.P. Bond durability of carbon fiber-reinforced polymer tendons embedded in high-strength concrete. *Journal of Composites for Construction*. 2018; **22**(5): 17p.

[21] Issa, M., Sen, R., and Amer, A. Comparative study of transfer length in fiberglass and steel pretensioned concrete member. *PCI Journal*. 1993; **38**(6): 52-63.

[22] Bischoff, P.H. Flexural response of concrete beams prestressed with AFRP tendons: numerical investigation. Discussion and Closures. *Journal of Composites for Construction.* 2012; **16**(3): 353-354.

[23] Imjai, T. Guadagnini, M., Garcia, R. and Pilakoutas, K. A practical method for determining shear crack induced deformation in FRP RC beams. *Engineering Structures* (2016); **126**(1): 353-364.